Comparison of adaptive filtering techniques for land surface data assimilation

W. T. Crow[1] and R. H. Reichle[2]

Received 30 January 2008; revised 13 May 2008; accepted 23 May 2008; published 15 August 2008.

[1] The accurate specification of modeling and observational error information required by data assimilation algorithms is a major obstacle to the successful application of a land surface data assimilation system. The source and statistical structure of these errors are often unknown, and poor assumptions concerning the relative magnitude of modeling and observation uncertainty degrade the quality of land data assimilation products. In theory, adaptive filtering approaches are capable of estimating model and observation error covariance information during the online cycling of a data assimilation system. To date, however, these approaches have not been widely applied to land surface models. Here, we implement and compare four separate adaptive filtering schemes in a data assimilation system designed to ingest remotely sensed surface soil moisture retrievals. Upon testing of each scheme via a synthetic twin data assimilation experiment, three of the four adaptive approaches are found to provide substantially improved soil moisture estimates. However, the specific model and observation characteristics of satellite-based surface soil moisture retrievals contribute to the relatively slow convergence of all schemes. Overall, results highlight the need to consider unique aspects of the land data assimilation problem when designing and/or evaluating the relative performance of adaptive filtering algorithms.

Citation: Crow, W. T., and R. H. Reichle (2008), Comparison of adaptive filtering techniques for land surface data assimilation, *Water Resour. Res.*, *44*, W08423, doi:10.1029/2008WR006883.

1. Introduction

[2] Hydrologic state and flux variable estimates derived from off-line land surface model simulations are valuable for a range of applications including: drought monitoring, numerical weather prediction, and hydrologic forecasting. Such estimates, however, are typically degraded by a range of error sources that afflict the modeling of land surface hydrologic conditions (e.g., improper parameter selection, errors in forcing data, and a simplistic representation of actual land surface processes and heterogeneity). Recently, a large number of studies have attempted to address these error sources through the assimilation of remotely sensed surface soil moisture estimates into a land surface model [e.g., *Walker and Houser*, 2001; *Reichle et al.*, 2002; *Crow and Wood*, 2003; *Reichle and Koster*, 2002, 2005; *Reichle et al.*, 2007; *Drusch*, 2007]. Such approaches are generally based on variants of a standard Kalman filter in which optimal weighting is applied to model forecasts and concurrent soil moisture retrievals to obtain a soil moisture analysis product with minimized error. The success of this approach is partially dependent on the accurate a priori specification of both a model noise covariance (representing uncertainty in model state forecasts) and an observation error covariance (representing uncertainty in remotely sensed soil moisture retrievals). In practice, however, such information is difficult to obtain and poor specification of these error quantities has been shown to degrade the performance of land data assimilation systems [*Reichle and Koster*, 2002; *Crow and Van Loon*, 2006; *Reichle et al.*, 2008].

[3] Adaptive filtering schemes refer to algorithms which attempt to estimate observation and model noise error covariances during the course of the filter analysis procedure. In this way, such schemes are able to automatically calibrate filters and prevent the application of excessive weight to either model background forecasts or updating observations. However, the wide range and variety of potential adaptive schemes and their strict assumptions and limitations complicate efforts to design an effective approach for any particular application. *Gelb* [1974], for example, cautions against adopting general adaptive filtering schemes on the basis of theoretical considerations and suggests that an application-specific heuristic strategy may be more effective. Such caution is likely to be particularly relevant for the use of adaptive methods in land data assimilation systems since land surface models differ significantly in structure and error characteristics relative to ocean and atmospheric models used in previous applications of adaptive filtering techniques to geophysical modeling. One key difference is that, unlike atmospheric forecast models, the physics of off-line land

[1]Hydrology and Remote Sensing Laboratory, Agricultural Research Service, U.S. Department of Agriculture, Beltsville, Maryland, USA.
[2]Global Modeling and Assimilation Office, Goddard Earth Sciences and Technology Center, NASA Goddard Space Flight Center, Greenbelt, Maryland, USA.

0043-1397/08/2008WR006883$09.00

surface models are fundamentally damped in nature [*Reichle et al.*, 2002]. As a result, uncertainty associated with the misspecification of initial conditions is progressively reduced over time and replaced with model errors that originate from inaccurate forcing data (e.g., precipitation) and model structural errors that impact the partitioning of the surface water balance.

[4] Because of land surface heterogeneity, land data assimilation systems must also contend with a lack of spatial stationarity in model error characteristics [*Yates et al.*, 2003]. By contrast, model error characteristics in atmospheric models are generally assumed to be spatially homogeneous [*Dee*, 1995]. This allows the use of simplified error models and the application of ergodic sampling techniques whereby spatial averaging is employed to improve the sampling of filtering diagnostics necessary to implement adaptive filtering approaches [*Mitchell and Houtekamer*, 1999]. Such ergodic sampling techniques are almost certainly inappropriate for land models applied to highly inhomogeneous landscapes. As a result, sampling issues surrounding the accurate estimation of filtering diagnostics, and the convergence of adaptive filters based on these diagnostics, are likely to be of prime concern for the application of adaptive filters to land data assimilation problems. Finally, the land surface state observations utilized in data assimilation (e.g., soil moisture and temperature) are often derived from relatively noisy and vertically incomplete remote sensing retrievals. Surface soil moisture retrievals from current passive microwave sensors, for example, sample only the top 1 to 3 cm of the soil column [*Jackson*, 1993]. Taken as a whole, these key differences imply that adaptive filtering techniques should be evaluated on the basis of their appropriateness for addressing challenges unique to land data assimilation.

[5] *Reichle et al.* [2008] take an initial step in this direction by developing an adaptive filtering procedure specifically for a land surface model. In the present paper, we apply their approach along with three additional adaptive filtering techniques to a soil moisture data assimilation problem and evaluate each approach on the basis of its ability to efficiently reconstruct known error covariance properties, and thus optimize ensemble Kalman filter (EnKF) performance, on the basis of information available during the operational cycling of a land data assimilation system. Because land data assimilation is typically performed using one-dimension filtering [*Reichle and Koster*, 2003], we restrict ourselves initially to a synthetic twin experiment methodology applied at a point scale. Instead, special emphasis is placed on the temporal convergence properties of filters and the degree to which particular adaptive filtering schemes are appropriate for a land data assimilation system.

2. Approach

[6] Our approach is based on a synthetic twin data assimilation experiment in which four separate adaptive filtering approaches are evaluated on their ability to filter noise which has been artificially introduced into a land surface model. Land surface modeling is discussed in section 2.1. The implementation of the four adaptive filtering approaches to the EnKF is described in sections 2.2 and 2.3, and section 2.4 summarizes the overall design of the synthetic twin experiment.

2.1. Land Surface Modeling

[7] The synthetic twin experiment employed here is based on the synthetic generation of soil moisture fields using the water and energy balance surface vegetation atmosphere transfer (WEB-SVAT) model. The model was developed by merging a force restore soil hydrology model [*Noilhan and Planton*, 1989; *Montaldo et al.*, 2001], with a two-layer vegetation/soil energy balance formulation utilizing a vertical canopy structure identical to that employed by the parallel version of the two-source model of *Norman et al.* [1995]. A full description of the model is given by *Crow et al.* [2008] and briefly summarized here.

[8] The Web-SVAT water balance approach is based on the vertical division of the soil column into surface and root zone reservoirs. These two reservoirs are modeled as vertically overlapping such that the surface zone constitutes the top fraction of the root zone. The temporal evolution of surface layer soil moisture (θ_{sz}) is given by

$$\frac{d\theta_{sz}}{dt} = \frac{B_1}{d_{sz}}\left[P_g - E_s\right] - \frac{B_2}{\tau}\left(\theta_{sz} - \theta_{eq}\right), \tag{1}$$

where P_g is precipitation throughfall, E_s direct soil evaporation, τ the frequency of diurnal variations (24 h), and d_{sz} the depth of the surface layer. Parameters B_1 and B_2 are soil texture and soil moisture dependent and θ_{eq} is a function of root zone soil moisture (θ_{rz}) such that the second term in (1) estimates the diffusive flux of water between the surface and bulk root zone [*Noilhan and Planton*, 1989; *Montaldo et al.*, 2001]. For the root zone, the analogous balance equation is

$$\frac{d\theta_{rz}}{dt} = \frac{1}{d_{rz}}\left[P_g - T - E_s - D\right], \tag{2}$$

where T is plant canopy transpiration, d_{rz} the root zone soil depth, and drainage D out the bottom of the root zone parameterized using soil saturated hydraulic conductivity K_s, porosity θ_{sat}, and the pore size distribution index parameter b as

$$D = K_s\left(\frac{\theta_{rz}}{\theta_{sat}}\right)^{2b+3}. \tag{3}$$

[9] Evaporative flux components in (1) and (2) are determined by solving a two-layer energy balance equation for canopy and surface aerodynamic skin temperatures, and partitioning between total precipitation and P_g is based on a simple canopy storage formulation [*Crow et al.*, 2008]. Here d_{sz} is set to 0.05 m and d_{rz} to 0.50 m. Soil hydrologic conductivity parameters are based on observed soil texture and look-up tables [*Noilhan and Planton*, 1989; *Cosby et al.*, 1984]. The WEB-SVAT model is well suited for our comparative study because of its parsimonious parameterization, computational efficiency, and the ease with which it can be linearized. While WEB-SVAT is simpler than most off-line land surface models (e.g., relative to schemes applied by *Dirmeyer et al.* [1999] or *Rodell et al.* [2005]), it still captures the key nonlinear attributes of more complex land surface models.

[10] The study domain is the Optimizing Production Inputs for Economic and Environmental Enhancements

(OPE^3) site located at the USDA-ARS Beltsville Area Research Center in Beltsville, Maryland. Vegetation cover consisted of cultivated corn, typically planted in May and harvested in October. Soil texture at the site is sandy loam [*Gish et al.*, 2005]. Meteorological variables (rainfall, air temperature, solar radiation, relative humidity and wind speed) are based on half-hourly observations made at the site during the 2001–2004 growing seasons. Long-term synthetic results are based on running the model on a half-hour time step and repeatedly cycling through the approximately 600 days of forcing data observations available at the site. Detailed validation results for the application of the Web-SVAT model to the OPE^3 site are available in work by *Crow et al.* [2008].

2.2. Ensemble Kalman Filtering

[11] The ensemble Kalman filter (EnKF) is based on utilizing a Monte Carlo ensemble of model realizations to obtain the error covariance information required by the Kalman filter update equation [*Evensen*, 1994]. Formally, the forecast step for a particular ensemble member i between times $t-1$ and t can be expressed as

$$x_{t,i-} = f\left(x_{t-1,i+}, q_{t,i}\right), \tag{4}$$

where $x_{t,i-}$ and $x_{t-1,i+}$ are the forecast state vector at time t and the analysis state vector at time $t-1$, respectively. The model perturbation vector $q_{t,i}$ represents uncertainty added to analysis state predictions during forecasting. Estimation of its covariance ($\mathbf{Q}_t$) is a key goal of adaptive filtering. Following forecasting, and the acquisition of a measurement at time t, the Kalman filter update equation produces a new analyzed state vector ($x_{t,i+}$)

$$x_{t,i+} = x_{t,i-} + \mathbf{K}_t\left(y_{t,i} - \mathbf{H}_t x_{t,i-}\right), \tag{5}$$

where $y_{t,i}$ denotes the a suitably perturbed [*Burgers et al.*, 1998] observation vector and $\mathbf{H}_t$ is an observation operator. The Kalman gain matrix $\mathbf{K}_t$ is given by

$$\mathbf{K}_t = \mathbf{P}_t\mathbf{H}_t^T\left(\mathbf{H}_t\mathbf{P}_t\mathbf{H}_t^T + \mathbf{R}_t\right)^{-1}, \tag{6}$$

where $\mathbf{P}_t$ is the forecast error covariance (sampled from individual realizations of $x_{t,i-}$ within the ensemble), $\mathbf{R}_t$ the observation error covariance, and the superscript T denotes a matrix transpose operator. The accurate estimation of $\mathbf{R}_t$ and $\mathbf{Q}_t$ is a critical precondition for the optimal specification of $\mathbf{K}_t$ and determines the weighting between model forecasts and new observations. In this study we focus on cases in which a priori guesses for $\mathbf{Q}_t$ and $\mathbf{R}_t$ are (intentionally) poorly chosen and then dynamically adjusted with adaptive filtering techniques.

[12] All results are based on the assimilation of synthetic surface soil moisture retrievals into the two-state (i.e., surface and root zone soil moisture) WEB-SVAT model at a single point that represents the OPE^3 site. Potential temporal variations in error covariances are not considered, and $\mathbf{Q}$ and $\mathbf{R}$ are assumed to be constant in time. As such, $\mathbf{H}_t \equiv H = (1,0)$, $\mathbf{K}_t$ reduces to the vector K_t (with the same dimension as x_t) and $\mathbf{R}$ simplifies to the constant scalar error variance R. We will also further assume that $\mathbf{Q}$ is of the form

$$\mathbf{Q} = \begin{pmatrix} Q & \alpha Q\rho \\ \alpha Q\rho & \alpha^2 Q \end{pmatrix},$$

where ρ is the correlation coefficient between perturbations applied to the surface and root zone soil moisture layers and α is the ratio of perturbation standard deviations for the root and surface zones. $\mathbf{Q}$ is assumed to capture the aggregate impact of all model errors (regardless of their source). This includes errors arising from uncertainty in surface meteorological forcings or land model parameters, which are not separately modeled here.

2.3. Adaptive Filters

[13] A commonly used diagnostic for adaptive filtering is the difference between observations and forecasts encountered during the application of (5)

$$v_t = E\left\{y_{t,i} - Hx_{t,i-}\right\}, \tag{7}$$

where $E\{\cdot\}$ is the ensemble mean operator. For the simple case examined here of a single observation (i.e., scalar $H\mathbf{P}_tH^T$ and R), v_t can be normalized as

$$\tilde{v}_t = E\{y_{t,i} - Hx_{t,i-}\}/\left(H\mathbf{P}_tH^T + R\right)^{1/2}. \tag{8}$$

[14] Linear filtering theory mandates that, for a properly parameterized filter, a $\tilde{v}_t$ time series should be mean zero, serially uncorrelated and have a temporal variance of one [*Gelb*, 1974].

2.3.1. Mehra Approach

[15] The adaptive filtering approach presented by *Mehra* [1970], hereafter referred to as the "Mehra" algorithm, is based on sampling the temporal variance (C_0) and lag-1 autocovariance (C_1) of the v_t time series defined by (7). Originally, the Mehra approach was developed for a linear forecast model $\mathbf{\Phi}$ updated with equally spaced observations (in time) and nonvarying error covariance parameters. For such systems, the background error covariance immediately before updating always reaches the same steady state value $\mathbf{P}_0$, which further implies a constant Kalman gain $K_0 = \mathbf{P}_0 H^T (H\mathbf{P}_0 H^T + R)^{-1}$. The Mehra approach then consists of a set of equations which offers a closed-form solution for $\mathbf{Q}$ and R. First, $\mathbf{P}_0H^T$ is computed with

$$\mathbf{P}_0H^T = \left[(H\mathbf{\Phi})^T(H\mathbf{\Phi})\right]^{-1}(H\mathbf{\Phi})^T(C_1 + H\mathbf{\Phi}K_0C_0) \tag{9}$$

followed by the (scalar) R as

$$R = C_0 - H\mathbf{P}_0H^T. \tag{10}$$

[16] Knowledge of C_0 and C_1 is also sufficient to define a single constraint on $\mathbf{Q}$

$$\begin{aligned} &H\mathbf{Q}\left(\mathbf{\Phi}^{-1}\right)^TH^T \\ &\quad = \left(\mathbf{P}_0H^T\right)^T\left(\mathbf{\Phi}^{-1}\right)H^T - H\mathbf{\Phi}\mathbf{P}_0H^T - H\mathbf{\Omega}\left(\mathbf{\Phi}^{-1}\right)^TH^T, \end{aligned} \tag{11}$$

where

$$\mathbf{\Omega} = \mathbf{\Phi}\left[-K_0\left(\mathbf{P}_0H^T\right)^T - \mathbf{P}_0H^TK_0^T + K_0C_0K_0^T\right]\mathbf{\Phi}^T. \tag{12}$$

[17] In our implementation of the Mehra approach, we divide the experiment period into discrete, nonoverlapping

N-day periods that each contain multiple updates via (5). The v_t time series within the jth such period is then sampled to obtain $C_{0,j}$ and $C_{1,j}$.

[18] Adaptation of the Mehra approach to the nonlinear WEB-SVAT requires several additional considerations. First, a unique single steady state gain K_0 will not exist when the EnKF is applied to a nonlinear model. Here, we pragmatically estimate $K_{0,j}$ for the jth N-day period by simply averaging time-varying values of K_t for each daily update within this period. Because the nonlinear WEB-SVAT model cannot be expressed in a time constant matrix $\mathbf{\Phi}$, we also approximate $\mathbf{\Phi}$ with a 2×2 matrix ($\mathbf{\Phi}'$) that contains a tangent linear approximation to the Web-SVAT model. Elements of $\mathbf{\Phi}'$ are then averaged within the jth N-day window to approximate $\mathbf{\Phi}_j$.

[19] At the end of the jth N-day period, $C_{0,j}$, $C_{1,j}$, $K_{0,j}$ and $\mathbf{\Phi}_j$ are input into (9) and (10) to obtain a new estimate of R, denoted with R'_j. Using (11) and (12), these inputs can also be used to estimate a single parameter within the $\mathbf{Q}$ matrix (Q'_j). Since each application of (9) to (12) for a given period j should yield unbiased estimates of both Q and R [*Mehra*, 1970], these new estimates are averaged with previously acquired values to obtain new a priori estimates of R and Q for the adaptive EnKF during time window $j + 1$

$$Q_{j+1} = 1/j \sum_{l=1}^{j} Q'_l \tag{13}$$

$$R_{j+1} = 1/j \sum_{l=1}^{j} R'_l. \tag{14}$$

2.3.2. Empirical Whitening

[20] As described above, the application of the closed-form Mehra algorithm to a nonlinear model is potentially problematic and may undermine the accuracy of its Q and R estimates. An alternative adaptive approach is therefore to use an iterative search technique and tune the ratio Q/R until a serially uncorrelated v_t time series is obtained. A white innovation time series is a fundamental property of an optimal filtering algorithm and indicates the extraction of all observational information in a single update step [*Gelb*, 1974]. Empirical approaches to such whitening are potentially more robust than the Mehra approach when applied to a nonlinear model.

[21] Here, two separate techniques will be used for empirically whitening the innovation time series. These techniques are applied separately as an alternative to the closed-form Mehra approach. The first whitening approach, referred to as "nudge whitening," is based on a simple rule-based updating. Starting from initial guesses for Q and R (Q_0 and R_0), the approach empirically updates the ratio $\Delta_j \equiv Q_j/R_j$ on the basis of the sign of the sampled lag-1 autocovariance C_1 of the v_t time series within the jth N-day window

$$\Delta_{j+1} = \begin{Bmatrix} \chi\Delta_j & C_{1,j} > 0 \\ \Delta_j & C_{1,j} = 0 \\ \chi^{-1}\Delta_j & C_{1,j} < 0 \end{Bmatrix},$$

where $\chi > 1$ is an empirical factor, chosen here as $\chi = 2$. Positive (negative) sampled values of $C_{1,j}$ indicate the filter is placing too little (much) weight on updating observations relative to background state predictions [see, e.g., *Crow and Bolten*, 2007]. The nudging procedure attempts to correct any such imbalance via empirical adjustments to the relative magnitude of Q and R.

[22] A competing updating approach, referred to here as "secant whitening," is to use a first-order secant root finder to estimate the value of Δ at which C_1 is zero (i.e., the v_t time series is serially uncorrelated). The secant whitening update is based on sampling C_1 from the v_t time series within discrete windows $j - 1$ and j to approximate the $j + 1$ value of Q_{j+1}/R_{j+1} as

$$\Delta_{j+1} \equiv Q_{j+1}/R_{j+1} = \Delta_j - \left(\Delta_{j-1} - \Delta_j\right)\left(C_{1,j-1} - C_{1,j}\right)^{-1}. \tag{15}$$

[23] Such an approach is more sophisticated than the nudging approach in that the magnitude of the update is based on a linear fitting to results for both the current and previous N-day window.

[24] For the derivation of new estimates of Q and R, the new estimate of Δ_j is combined with a constraint on the total error C_0 equal to the sum of the model and observation error covariance (10). Assuming that the ratio Q_j/R_j is close to optimal, and therefore C_1 near zero, R_{j+1} for both whitening approaches can be approximated (for this scalar case) by combining (6), (8) and (10) to yield

$$R'_{j+1} \simeq C_{0,j}\left(1 - HK_{0,j}\right) \tag{16}$$

or equivalently,

$$R'_{j+1} \simeq \tilde{C}_{0,j} R_j, \tag{17}$$

where $\tilde{C}_{0,j}$ is the variance of $\tilde{v}_t$ sampled within the jth N-day window. The error variance Q'_{j+1} is then estimated as

$$Q'_{j+1} = R'_{j+1}\Delta_{j+1}. \tag{18}$$

[25] Here, a final moving average procedure is added to smooth estimates prior to their insertion back into the adaptive EnKF

$$Q_{j+1} = Q'_{j+1}/2 + Q_j/2 \tag{19}$$

$$R_{j+1} = R'_{j+1}/2 + R_j/2. \tag{20}$$

2.3.3. Desroziers Approach

[26] The approach of *Desroziers et al.* [2005], hereafter referred to as the "Desroziers" algorithm, is based on the specification of two additional filtering diagnostics, w_t and u_t, to complement v_t. The analysis departure w_t is defined as the difference between the predicted and actual observations after Kalman updating

$$w_t = E\left\{y_{t,i} - Hx_{t,i+}\right\}. \tag{21}$$

[27] The observation analysis increment u_t represents the impact of the update in observation space

$$u_t = E\left\{H\left(x_{t,i+} - x_{t,i-}\right)\right\}. \tag{22}$$

[28] Following *Desroziers et al.* [2005], these diagnostics can be combined with v_t to yield two separate constraints

$$E\left[u_t v_t^T\right] = H\mathbf{P}_t H^T \tag{23}$$

$$E\left[w_t v_t^T\right] = R, \tag{24}$$

where $E[\cdot]$ denotes the temporal mean operator. Choosing values of Q and R that respect these two constraints should lead to optimized filter performance.

[29] *Reichle et al.* [2008] derive an operational procedure for the online tuning of Q and R to meet the constraints imposed by (23) and (24). Their adaptive filter attempts to estimate the ratio between true input error variances and (potentially poor) initial guesses for such variances (R_0 and Q_0) by comparing assumed values of $H\mathbf{P}_t H^T$ (which vary as a function of Q) with values of $E[u_t\, v_t^T]$ obtained during the integration of an EnKF, and, simultaneously, by comparing assumed values of R with corresponding values of $E[w_t\, v_t^T]$. To this end, they define a moving average operator ($\mathbf{MA}[\cdot]$) of the form $\mathbf{MA}[x]_t = (1 - \delta)\mathbf{MA}[x]_{t-1} + \delta \cdot x_t$ with an ad hoc choice of $\delta = 0.02$. This operator is then used to separately sample terms in (23) and (24) and calculate the ratios

$$f_{Q,t} = \beta \mathbf{MA}\left[uv^T\right]_t / \mathbf{MA}\left[H\mathbf{P}_t H^T\right]_t \tag{25}$$

$$f_{R,t} = \mathbf{MA}\left[wv^T\right]_t / \mathbf{MA}[R]_t. \tag{26}$$

[30] The factor β will be explained below. Because of residual noise in the moving average estimates, $f_{Q,t}$ and $f_{R,t}$ are restricted to the interval $[(1 + d)^{-1}, (1 + d)]$, with $d = 0.005$. The restricted scaling factors $\tilde{f}_{Q,t}$ and $\tilde{f}_{R,t}$ are then used to adjust the most recent estimates of Q and R via

$$Q_{t+1} = \tilde{f}_{Q,t} Q_t \tag{27}$$

$$R_{t+1} = \tilde{f}_{R,t} R_t. \tag{28}$$

[31] In practice, this means Q_t and R_t are decreased or increased by only a relatively small fraction at each update time, no matter how far the originally calculated fractions $f_{Q,t}$ and $f_{R,t}$ are from unity. In addition, Q_{t+1}/Q_0 and R_{t+1}/R_0 are restricted to the interval [0.01, 100], and, consequently, error covariances are not allowed to stray more than 2 orders of magnitude from the initial estimates. *Reichle et al.* [2008] also introduced the tuning parameter β in (25) to address the generally nonlinear relationship between the model error covariance $\mathbf{Q}$ and the forecast error covariance $\mathbf{P}$. The ad hoc value of $\beta = 1.06$ tuned by *Reichle et al.* [2008] will also be used here. In the following section, a sensitivity analysis will be conducted to determine the impact of variations in β on key results. Note that, in contrast to the Mehra and secant whitening approaches in which Q and R values are updated only upon completion of discrete N-day periods, the Desroziers approach continuously updates Q and R after every daily observation.

2.4. Synthetic Twin Experiment

[32] The four adaptive filtering schemes described above (i.e., the Mehra, nudge whitening, secant whitening and Desroziers approaches) are evaluated on the basis of their performance in a synthetic twin experiment. Here, the true model noise error covariance $\mathbf{Q}_{\text{true}}$ is defined by assuming $\alpha = 0.30$, $\rho = 0.70$ and $\text{Sqrt}(Q_{\text{true}}) = 0.05$ vol/vol, where all soil moisture error values are given in terms of volumetric moisture content (i.e., the volume of water per total volume of soil). During adaptive filtering, both α and ρ are assumed known. Consequently, deriving the full $\mathbf{Q}_{\text{true}}$ matrix reduces to the problem of identifying the scalar Q_{true} (see section 2.2).

[33] Using daily additive q_t perturbations with covariance $\mathbf{Q}_{\text{true}}$, a single integration of the Web-SVAT model is perturbed and its soil moisture output defined as "truth." Surface soil moisture θ_{sz} estimates from this truth run are then perturbed with additive noise, statistically consistent with a specified true R (R_{true}), to form a set of daily observations. Unless otherwise specified, $\text{Sqrt}(R_{\text{true}}) = 0.04$ vol/vol. These daily observations are then reassimilated into an unperturbed WEB-SVAT model integration using a 25-member ensemble Kalman filter (EnKF). EnKF estimates are derived from averaging soil moisture across the ensemble and evaluated on the basis of their ability to recreate the soil moisture results from the "truth" simulations.

[34] To test a specific adaptive filtering approach, the EnKF portion of this synthetic experiment is replicated across a stratified grid of guesses for the magnitude of $\text{Sqrt}(Q_{\text{true}})$ and $\text{Sqrt}(R_{\text{true}})$. Such initial estimates are referred to as $\text{Sqrt}(Q_0)$ and $\text{Sqrt}(R_0)$. Each adaptive filtering approach is then evaluated on the basis of its ability to adaptively correct inaccurate $\text{Sqrt}(Q_0)$ and $\text{Sqrt}(R_0)$ estimates and converge upon Q_{true} and R_{true}. Using growing season meteorological observations at the OPE^3 site, each approach is tested over a period of 3000 days in which daily (synthetic) observations of surface soil moisture are continuously assimilated. Unless otherwise stated, a sampling period N of 50 days will be used for the Mehra, secant whitening and nudge whitening approaches.

3. Results

[35] For the synthetic twin experiment outlined above, Figure 1 describes the sensitivity of EnKF results (derived without adaptive filtering) to the accuracy of Q_0 and R_0 estimates. Coordinate values of $\text{Sqrt}(Q_0)$ and $\text{Sqrt}(R_0)$ in Figure 1 represent assumed error values in units of volumetric soil moisture and the surface height captures the long-term root-mean-square error (RMSE) accuracy of EnKF soil moisture estimates associated with these assumptions. True values of $\text{Sqrt}(Q)$ and $\text{Sqrt}(R)$ ($\text{Sqrt}(Q_{\text{true}})$ and $\text{Sqrt}(R_{\text{true}})$) are indicated by white crosses. To avoid spin-up effects, surface RMSE values in Figure 1 are calculated by discarding the first 1000 days of the simulations and sampling RMSE between days 1001 and 3000. Transient convergence characteristics during the first 1000 days of the simulation will be discussed later. Both the long-term RMSE for θ_{sz} (Figure 1a) and θ_{rz} (Figure 1b) display a broad minimum which encompasses both $\text{Sqrt}(Q_{\text{true}})$ and $\text{Sqrt}(R_{\text{true}})$, thus confirming that optimal filter performance is associated with accurate error covariance assumptions [*Crow and Van Loon*, 2006; *Reichle et al.*, 2008].

[36] Open loop results (not shown) capture the uncorrected impact of model error $\mathbf{Q}_{\text{true}}$ prior to the application of the EnKF. For this combination of $\text{Sqrt}(Q_{\text{true}})$ and $\text{Sqrt}(R_{\text{true}})$, open loop RMSE values of 0.056 and 0.035 vol/vol are obtained for θ_{sz} and θ_{rz}, respectively. The RMSE surface in Figure 1 falls below these open loop error levels for nearly all choices of $\text{Sqrt}(Q_0)$ and $\text{Sqrt}(R_0)$; however, as in the work by *Reichle et al.* [2008], the impact of poorly estimating Q and R can be large enough such that the EnKF estimates are worse than the open loop estimates (see, e.g., the bottom right-hand corner of Figures 1a and 1b).

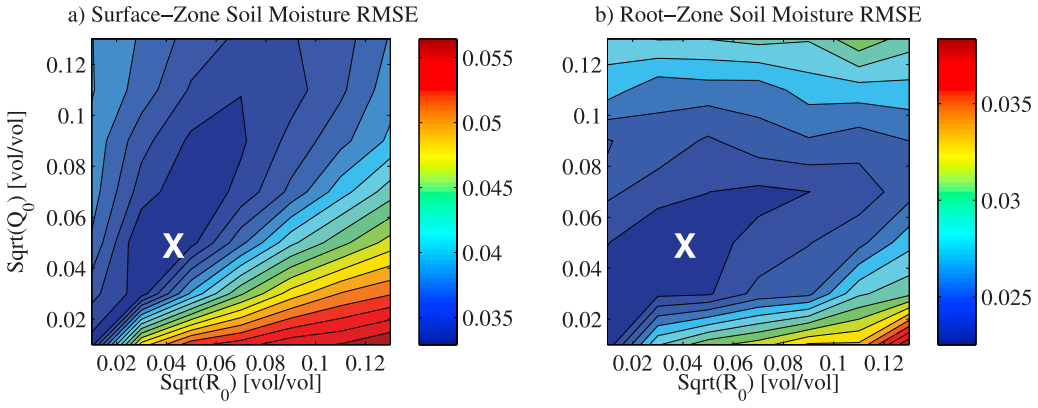

Figure 1. Contour plots of variations in (a) EnKF θ_{sz} and (b) EnKF θ_{rz} RMSE as a function of Sqrt(Q_0) and Sqrt(R_0) for the case of no adaptive filtering with Sqrt(Q_{true}) = 0.05 vol/vol and Sqrt(R_{true}) = 0.04 vol/vol (white crosses).

[37] In theory, the application of adaptive filtering schemes should improve results in Figure 1 by correcting initially poor estimates of Q and R. For all four adaptive schemes presented in section 2 (i.e., the Mehra, Desroziers, secant whitening and nudge whitening approaches), Figure 2 demonstrates this potential by plotting the temporal evolution of Q and R estimates as each adaptive filtering approach is run online with the EnKF. Each symbol in Figure 2 represents a single realization of an entire 25-member adaptive EnKF run. Black plus signs capture the stratified pattern of Sqrt(Q_0) and Sqrt(R_0) used to initialize each realization. A clear pattern of convergence toward Q_{true} and R_{true} (represented by the single black cross in each plot) can be observed for all four adaptive filtering approaches. The improved calibration of Q and R values captured in Figure 2 should enhance the performance of the EnKF relative to the baseline case in Figure 1 in which (potentially poor) initial estimates of Q and R are not adaptively updated.

[38] Figures 3 and 4 explicitly capture the improvement in EnKF θ_{sz} and θ_{rz} estimates for all four filtering approaches. As in Figure 1, coordinate values of Sqrt(Q_0) and Sqrt(R_0) represent initial assumptions concerning Q_{true} and R_{true}. However, the plotted surface height now represents the change in EnKF RMSE (defined as adaptive EnKF RMSE minus the nonadaptive EnKF RMSE) realized upon implementation of each adaptive filtering technique. The bold line in each plot represents the zero contour separated areas of degraded results (indicated in red) from areas in which application of the adaptive filter improves EnKF results. Negative contour heights in Figures 3 and 4 indicate that all four adaptive approaches are generally able to improve upon uncorrected results in which Q_0 and R_0 are not updated (Figure 1). Unsurprisingly, net reductions in RMSE tend to be greatest for values of Q_0 and R_0 that differ significantly from Q_{true} and R_{true} (see white crosses in Figures 3 and 4). When initial estimates of Q and R are assumed to be relatively good (i.e., Q_0 and R_0 are near Q_{true} and R_{true}), it is possible for the adaptive filter to slightly degrade EnKF results. Such degradation is particularly clear for Mehra θ_{sz} results plotted in Figure 3a. For a broad area of Figure 3a in which $Q_0 > R_0$, application of the Mehra algorithm slightly reduces the accuracy of EnKF surface soil moisture predictions relative to a baseline case of no adaptive filtering. However, these problems do not appear to extend into root zone results plotted in Figure 4, where the Mehra approach performs relatively well.

[39] An additional qualitative difference among the four approaches is the relatively poor performance of the secant whitening algorithm. This difference is clearest in the bottom right corner of Figures 3c and 4c. Here the other

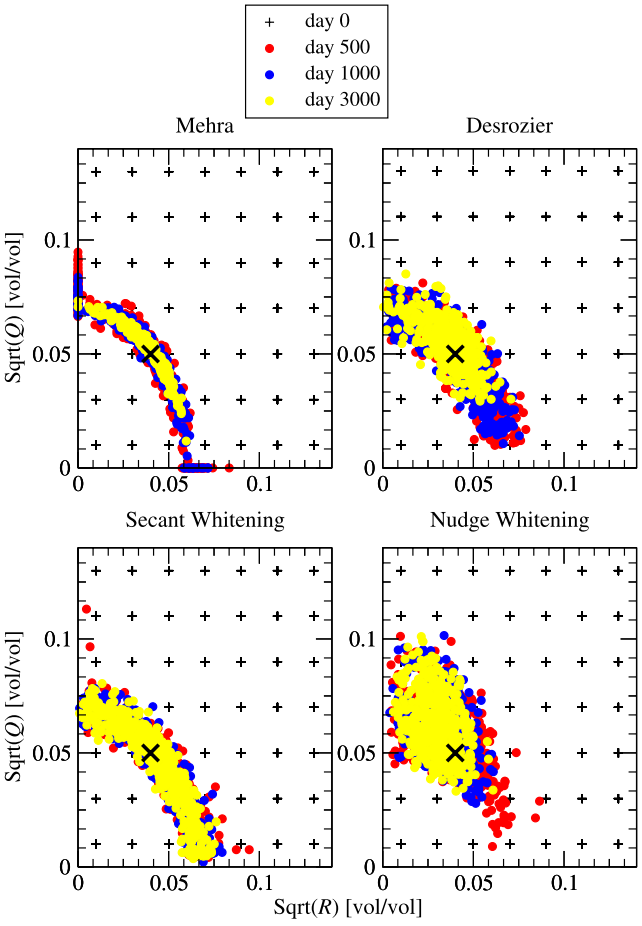

Figure 2. Observed convergence of Q and R estimates obtained from the Mehra, Desroziers, secant whitening, and nudge whitening adaptive filtering approaches for various daily time steps. The black crosses represent Sqrt(Q_{true}) and Sqrt(R_{true}).

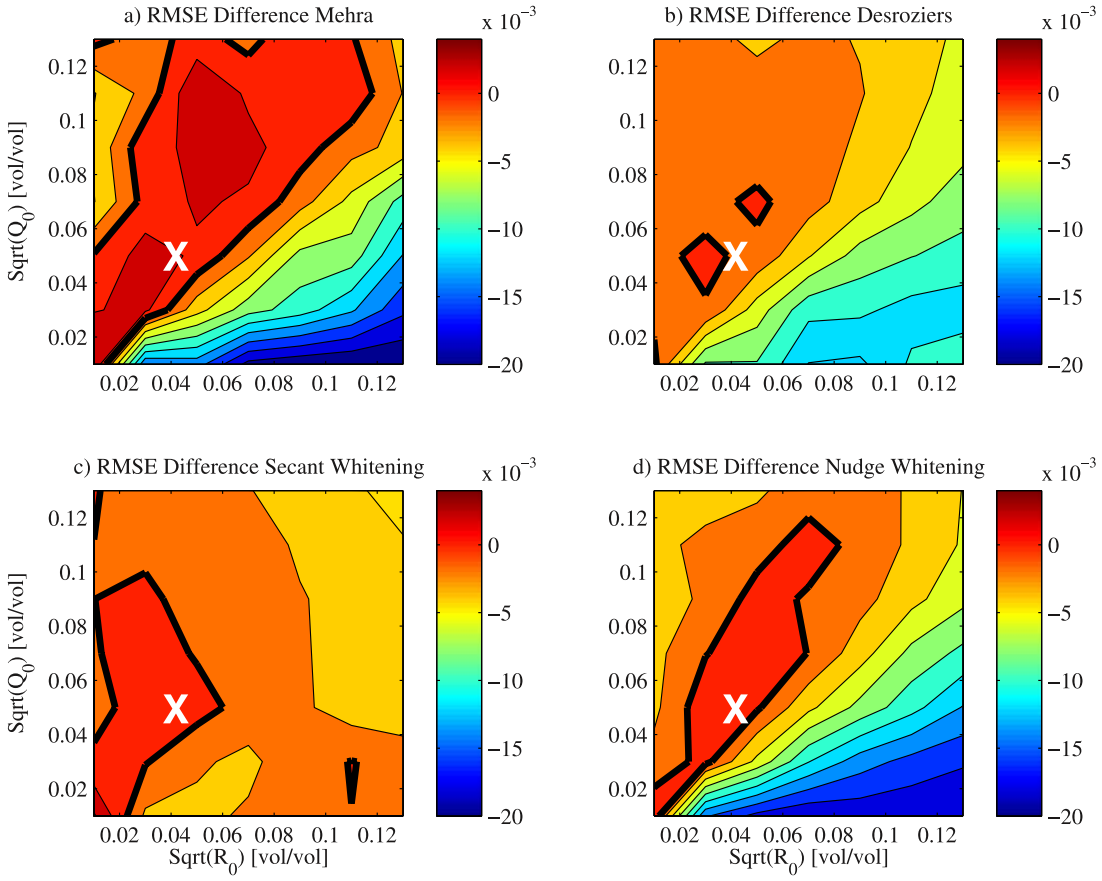

Figure 3. The impact of adaptive filtering on surface zone soil moisture (θ_{sz}) RMSE as a function of Q_0 and R_0 for the case of the (a) Mehra, (b) Desroziers, (c) secant whitening, and (d) nudge whitening adaptive filtering approaches, where Sqrt(Q_{true}) = 0.05 vol/vol and Sqrt(R_{true}) = 0.04 vol/vol (white crosses). The thick black line indicates the zero contour (indicating no RMSE change upon implementation of an adaptive filter).

three approaches are able to realize significant reductions in EnKF soil moisture RMSE; however, the secant whitening approach is limited to marginal improvement (or even slight degradation) relative to the baseline case of no adaptive filtering. This lack of improvement appears to arise from the difficulty of obtaining accurate updates using a two-step secant root finder in the presence of significant sampling uncertainty in $C_{1,j}$ estimates. The impact of such uncertainty on the difference between $C_{1,j-1}$ and $C_{1,j}$, required by the secant root finder in (15) to predict subsequent updates, impairs the ability of the root finder to skillfully update error covariance estimates and thus inhibits the convergence of the approach. As a result, the secant whitening approach will not be considered in subsequent results.

3.1. Adaptive Convergence

[40] As noted in section 1, a key aspect of adaptive filtering (particularly for land models) is the speed at which adaptive filtering estimates of Q and R converge upon true values. Figure 5 examines this issue by plotting the time series of Sqrt(Q) and Sqrt(R) RMSE obtained by sampling the mean squared difference (at each time step) between estimated and true error covariance values for all initial choices of Q_0 and R_0. Results are shown for all three remaining adaptive filtering approaches (the Mehra, Desroziers, and nudge whitening techniques). For comparison, Figure 5 also plots time series results for the case of no adaptive filtering. All three approaches clearly improve upon the case of no adaptive filtering. Among the adaptive filtering approaches, the Mehra algorithm produces the lowest eventual R and Q RMSE. However, the relative superiority of the Mehra approach is small and emerges only after the assimilation of about 2000 daily observations (Figures 5a and 5b). During earlier portions of the synthetic twin experiment, both the nudge whitening and the Desroziers approach produce superior estimates of Q_{true} and R_{true}. Figure 5c plots the analogous time series for WEB-SVAT θ_{rz} RMSE. As in Figures 5a and 5b, the error is based on sampling across all initial choices for Q_0 and R_0. To improve its readability, the RMSE time series in Figure 5c is smoothed within a 150-day window prior to plotting. The initially poor specification of Q and R seen in the Figures 5a and 5c clearly hampers the early performance of the Mehra approach with regards to θ_{rz} estimation. However, after a lengthy convergence period, the Mehra approach is able to converge upon a slightly more optimal filter calibration than either the Desroziers or nudge whitening approach.

[41] Despite its eventual accuracy, the slow convergence rate of the Mehra algorithm in Figure 5 is striking. It is useful to consider what aspects of the land data assimilation problem contribute to this difficulty. To this end, we regenerated Figure 5 for the case of a purely linear model,

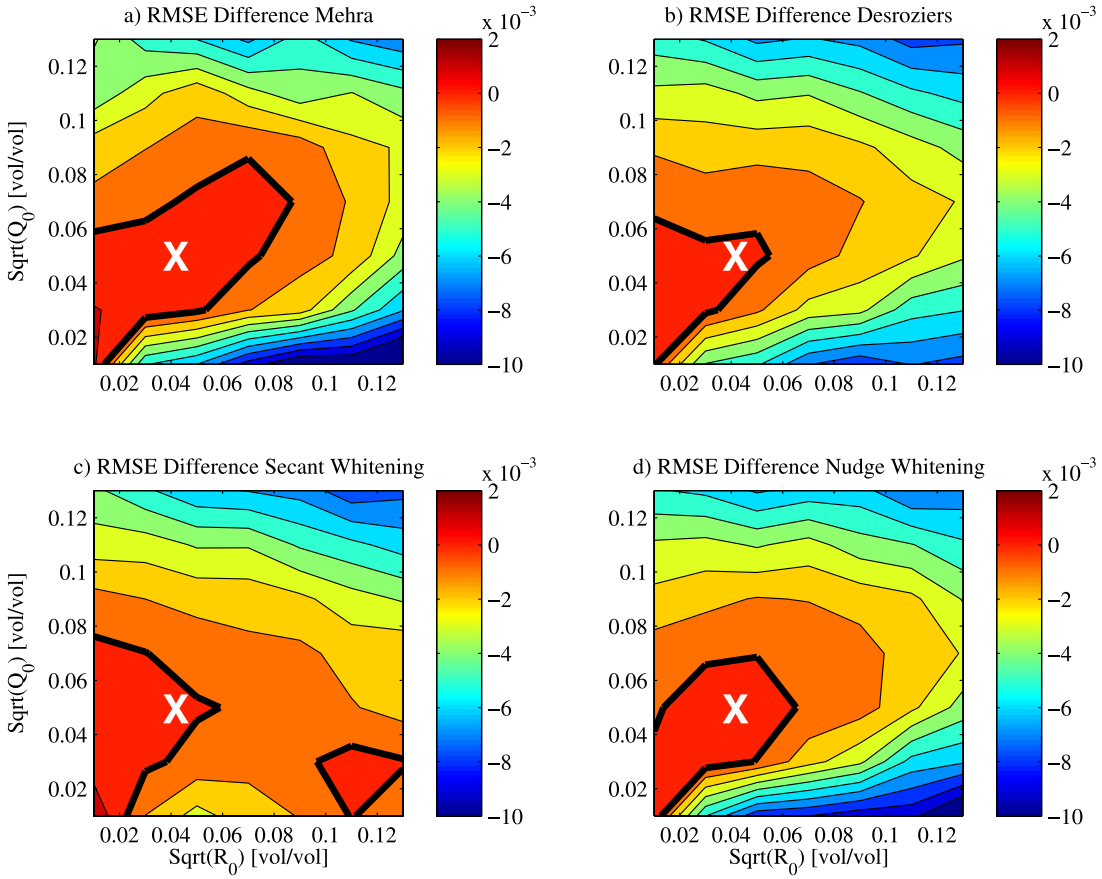

Figure 4. The impact of adaptive filtering on root zone soil moisture (θ_{rz}) RMSE as a function of Q_0 and R_0 for the case of the (a) Mehra, (b) Desroziers, (c) secant whitening, and (d) nudge whitening adaptive filtering approaches, Sqrt(Q_{true}) = 0.05 vol/vol and Sqrt(R_{true}) = 0.04 vol/vol (white crosses). The thick black line indicates the zero contour (indicating no RMSE change upon implementation of an adaptive filter).

calibrated to approximate WEB-SVAT soil moisture estimates, and found qualitatively similar results (not shown), suggesting that WEB-SVAT nonlinearities do not significantly contribute to the slow rate of convergence. In addition, because the Mehra approach is not based on an iterative search, its rate of convergence is relatively insensitive to variations in Q_0 and R_0. Instead, the problem appears to originate from properties of the assimilated observations themselves. Soil moisture observations assimilated into land surface models are, in actuality, retrievals based on relatively complex inverse radiative transfer modeling. Consequently, they are prone to high levels of observation error, potentially up to and greater than Sqrt(R_{true}) = 0.06 vol/vol for densely vegetated areas, which can overwhelm modest autocorrelation signals associated with poorly calibrated filters (and therefore weaken the conceptual basis of adaptive filtering updates). This is demonstrated in Figure 6a where the ability of the Mehra approach to converge on accurate Q levels is significantly degraded (enhanced) by an increase (decrease) in R_{true}.

[42] Remotely sensed retrievals of surface soil moisture are also limited by restrictions in the vertical penetration depth of microwave observations. A lack of vertical support for measurements effectively limits the temporal memory present in surface soil moisture retrievals and thus the extent of temporal autocorrelation present in background errors. This is critical since the contrast between autocorrelated errors in background WEB-SVAT soil moisture estimates (due to soil moisture memory) and the purely uncorrelated error assumed for surface soil moisture retrievals is the basis on which the Mehra algorithm simultaneously estimates both Q and R. This basis is effectively weakened if the amount of memory present in the observed surface soil moisture state is reduced. Figure 6b plots cases where the vertical depth of the top WEB-SVAT soil moisture layer used is systematically varied during the synthetic twin experiment. Results in Figure 6 confirm that better Mehra algorithm convergence can be achieved if observations are assumed to originate from a thicker surface soil moisture layer.

3.2. Enhancing Convergence

[43] Unfortunately, the observation characteristics discussed in connection with Figure 6 are fixed attributes of remotely sensed surface soil moisture retrievals that cannot be modified in real data applications. Several aspects of the adaptive filtering approaches introduced in section 2, however, can be modified in an operational environment. One possibility is changing the length of the estimation period used to sample C_0 and C_1 in the Mehra and nudge whitening approaches. Results for the Mehra approach display markedly little sensitivity to the length of the sampling period N (Figure 7a). The reduced sampling uncertainty afforded by a

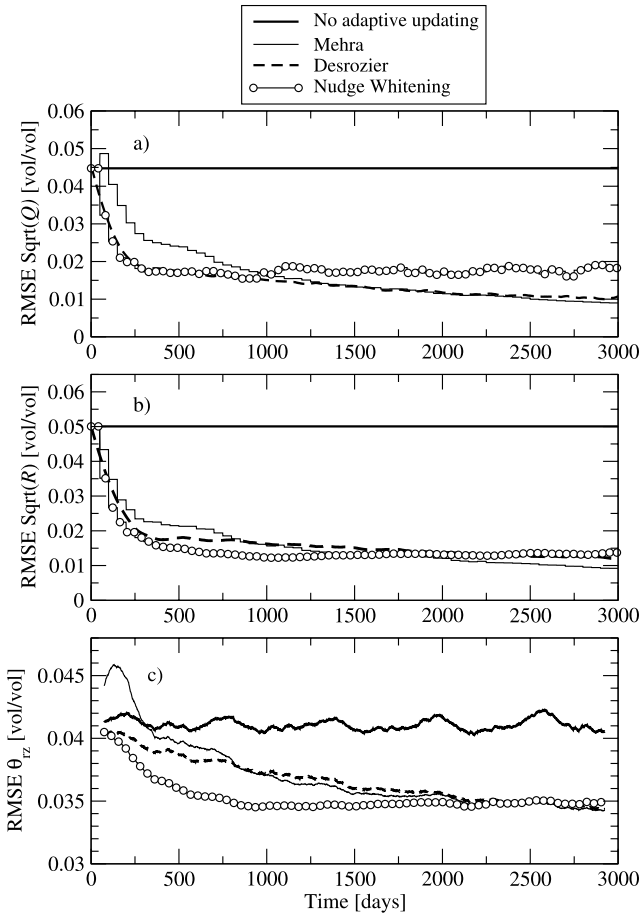

Figure 5. Time series of (a) predicted Sqrt(Q) RMSE, (b) predicted Sqrt(R) RMSE, and (c) EnKF θ_{rz} RMSE for various adaptive filtering strategies. Results are based on sampling across a stratified range of Sqrt(Q_0) and Sqrt(R_0). Time series results in Figure 5c have been smoothed with a 150-day moving average window.

larger N is canceled by the decrease in the frequency of updates to either Q or R required by a longer sampling period. Slightly more sensitivity to N is noted for the nudge whitening approach. Here, a lower value for N leads to a faster rate of convergence; however, it also increases the eventual Q RMSE level that the adaptive filter is able to converge to (Figure 7b).

[44] An alternative possibility is to constrain noisy Q and R estimates within predefined bounds. For instance, since the variance C_0 represents the aggregate impact of model observation and modeling error, it provides an upper bound for both Q and R. Likewise, by definition, both error variances must be positive. Consequently, the following two constraints can be implemented for both the Mehra and nudge whitening approaches

$$Q'_{j+1} = \mathrm{Max}\left[0, \mathrm{Min}\left(Q'_{j+1}, C_{0,j}\right)\right] \tag{29}$$

$$R'_{j+1} = \mathrm{Max}\left[0, \mathrm{Min}\left(R'_{j+1}, C_{0,j}\right)\right] \tag{30}$$

prior to updating using (13) and (14) (for the Mehra approach) or (19) and (20) (for the nudge whitening approach).

[45] Figure 8 shows that, at least for default values of Sqrt(Q_{true}) = 0.05 vol/vol and Sqrt(R_{true}) = 0.04 vol/vol, implementation of these constraints leads to dramatic improvement in the temporal convergence of Q values for the Mehra approach. Qualitatively similar results (not shown) are obtained for R. This implies that a large portion of the slow convergence for the Mehra approach in Figure 5 is attributable to variability originating from physically unrealistic estimates of Q' and R'. However, this benefit comes at a cost of reducing the robustness of the approach. While (29) and (30) are effective for cases in which R_{true} and Q_{true} are approximately equal, physically unrealistic values eliminated by these constraints play a role in ensuring adequate convergence in cases where total error covariance is disproportionately apportioned to either R or Q. For instance, in a low-Q_{true} and high-R_{true} case, negative Q' values, while physically unrealistic, are required to ensure that individual Q' estimates are unbiased and therefore converge to Q_{true} upon temporal averaging. Consequently, the truncation of negative Q' values to zero via (29) introduces a positive bias in eventual estimates of Q. While the application of the constraints (29) and (30) enhances the speed at which the Mehra approach converges, it introduces biases which hamper the ultimate fidelity of the approach. Figure 9 illustrates the potential trade-off. As a result, the constrained

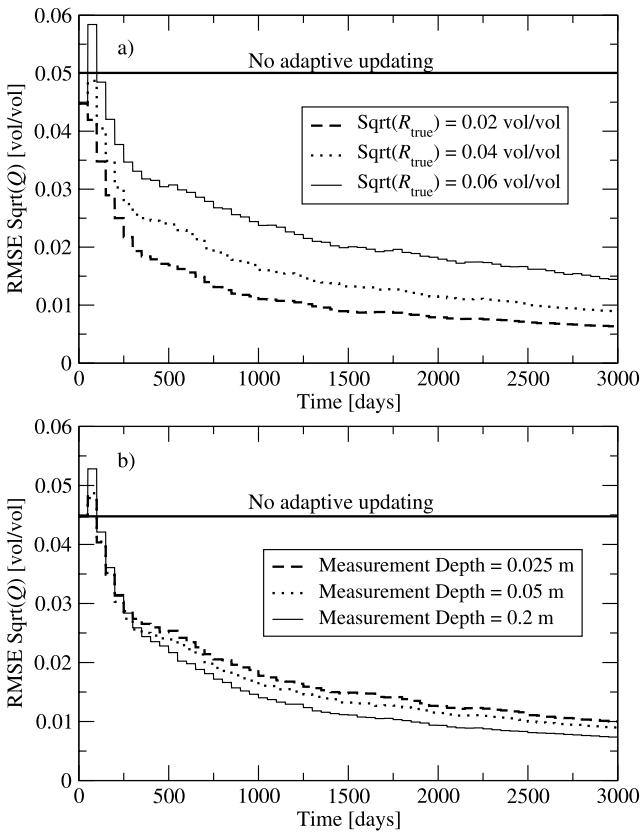

Figure 6. Impact of (a) R_{true} and (b) the vertical measurement depth of surface soil moisture retrievals on the convergence of Q estimates obtained using the Mehra approach.

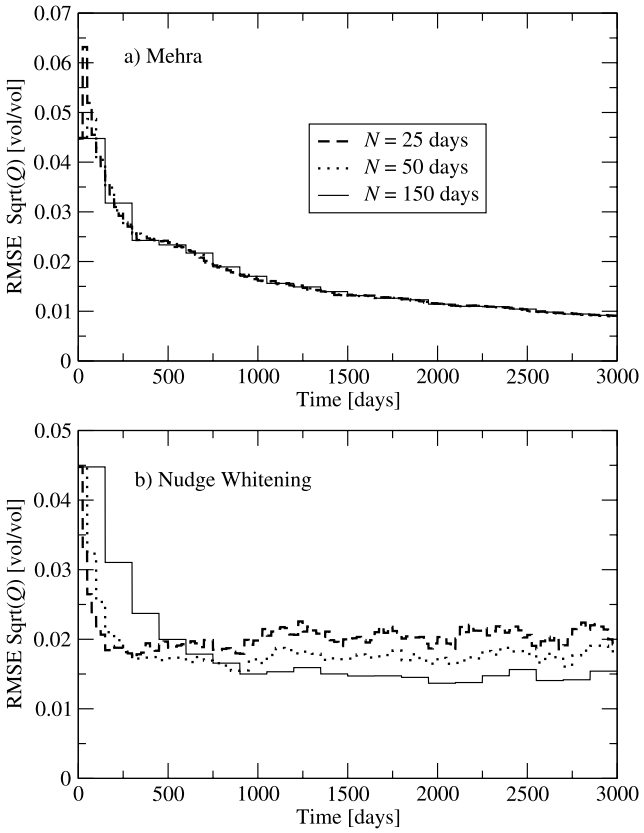

Figure 7. Impact of sampling period length N on the rate of convergence seen in Q estimates obtained from the (a) Mehra and (b) nudge whitening adaptive filtering approaches.

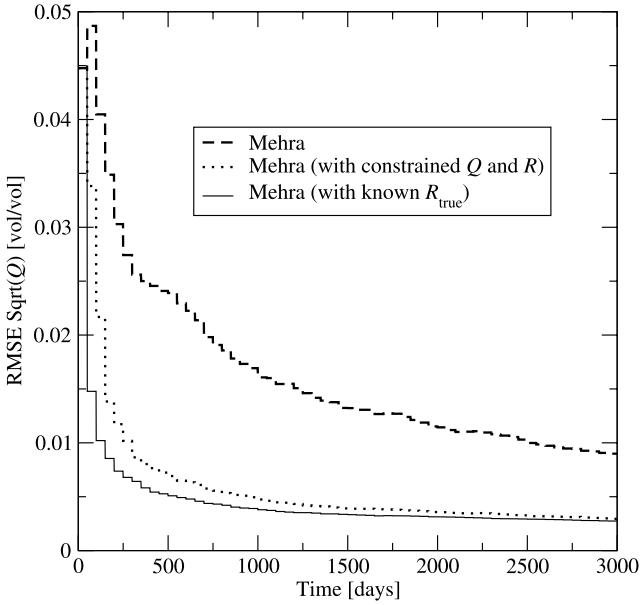

Figure 8. The Q convergence of the original Mehra approach, the Mehra approach in which Q and R estimates are constrained via application of (29) and (30), and the Mehra approach in which R_{true} is assumed to be known.

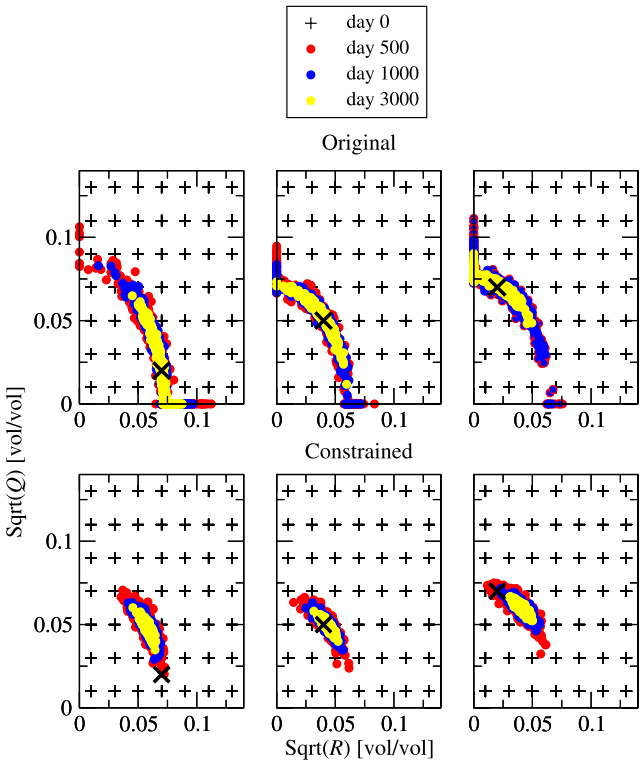

Figure 9. The observed convergence of Q and R estimates obtained from the original and constrained Mehra approaches for a variety of Sqrt(Q_{true}) and Sqrt(R_{true}) (black crosses), via (29) and (30), for various daily time steps.

Mehra approach performs well (relative to the original Mehra approach) for the case $R_{\text{true}} \sim Q_{\text{true}}$ (middle plot) but does not converge accurately for $Q_{\text{true}} \ll R_{\text{true}}$ (far left plots) or $Q_{\text{true}} \gg R_{\text{true}}$ (far right plots). Qualitatively analogous results are obtained for the nudge whitening approach (not shown).

[46] A final possibility is to assume R_{true} is known and reduce the adaptive filtering problem to the estimation of Q_{true} only. Assuming direct observation of surface soil moisture retrievals (i.e., H = (1,0)), accurate a priori estimates of R_{true} can be used to estimate $\mathbf{P}_0 H^{\text{T}}$ via (10). Relative to more uncertain estimates of $\mathbf{P}_0 H^{\text{T}}$ obtained from (9) without direct knowledge of R_{true}, these new values can be used to obtain a more precise approximation of Q_{true} via (11). This impact is clearly seen in Figure 8 where an assumption of perfectly known R_{true} substantially improves the performance of the Mehra algorithm. Unlike the constrained variant of the Mehra approach described above, additional synthetic twin experiments (not shown) demonstrate that the effectiveness of this modification is not limited to a certain range of Q_{true}.

3.3. Tuning of the Desroziers Method

[47] A potentially problematic aspect of the Desroziers approach as implemented by *Reichle et al.* [2008] lies in the need to introduce the ad hoc scaling parameter β in (25) to ensure the robust performance of the algorithm. Up to this point, all Desroziers results have been based on the choice of β = 1.06 suggested by *Reichle et al.* [2008]. Here this issue is examined in greater detail by comparing the

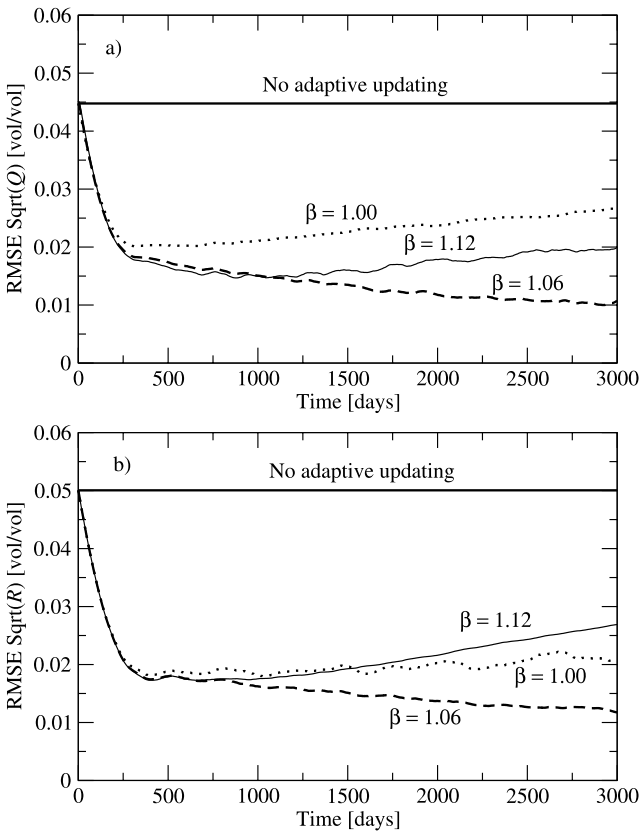

Figure 10. Impact of the β parameter on the convergence of (a) Q and (b) R obtained using the *Reichle et al.* [2008] implementation of the Desroziers approach.

performance of the algorithm for various choices of β. Figure 10 compares the adaptive Q and R convergence observed for β = 1.00, 1.06 and 1.12. Maximum convergence (i.e., lowest Q and R RMSE) for both Q and R is observed for the choice of β = 1.06 suggested by *Reichle et al.* [2008]. However, slightly higher or lower choices of β can lead to the long-term drift of estimated Q and R away from their true values and potentially unstable adaptive filtering performance.

[48] A more detailed analysis (not shown) indicates that the β factor impacts the ratio Q/R in long-term adaptive filtering results with lower β associated with lower estimated Q/R. This is critical because in linear filtering theory, it is this ratio which controls the manner in which relative weighting is applied to model background and new observations during implementation of the EnKF. The approximate correspondence of optimal β values found here and in the work by *Reichle et al.* [2008] is somewhat surprising given that completely different land surface models (and different synthetic twin experimental setups) are employed in each case. This may imply that optimal values of β are, to at least to a first approximation, model independent. However, further study is required to understand the theoretical basis of β and potential difficulties encountered in its robust estimation.

4. Summary and Conclusions

[49] The application of an EnKF to a land surface model requires that the filter be provided error covariance estimates of both modeling noise (Q) and observation uncertainty (R) (Figure 1). The true values of these error parameters, however, depend on the application at hand and are typically difficult to estimate a priori. Here, four separate adaptive filtering approaches (described in section 2 and referred to as Mehra, Desroziers, secant whitening and nudge whitening approaches) are evaluated on the basis of their ability to recover unknown scalar Q and R magnitudes during the online implementation of the EnKF to a surface soil moisture data assimilation problem (Figure 2). Out of the four approaches, the secant whitening adaptive filtering method performs the worst with regards to enhancing model soil moisture estimates (Figures 3 and 4). Of the three more successful adaptive filtering approaches, the Mehra approach provides superior long-term convergence to true Q and R (Figures 5a and 5b) and therefore slightly improved EnKF performance (Figure 5c). The successful application of the Mehra approach to the nonlinear WEB-SVAT model is noteworthy. The relatively crude approximations required by this application (see section 2.3.1) would likely be inappropriate for a highly nonlinear atmospheric model containing unstable modes but appear to be sufficient for a land surface model with fundamentally damped physics.

[50] Despite this success, the utility of the Mehra approach is reduced by its relatively slow rate of convergence (Figure 5). Such slow convergence is likely to be particularly problematic for the application of adaptive filtering techniques to land surface models since typical land surface spatial heterogeneity suggests that model error parameters should vary laterally over a given domain. Consequently, ergodic assumptions, in which temporal sampling difficulties are eased through spatial sampling, cannot be applied with confidence. These difficulties are exacerbated by the shallow and noisy nature of soil moisture retrievals derived from microwave remote sensing which retard the adaptive convergence of the Mehra approach (Figure 6). The convergence speed of the Mehra approach does not improve upon lengthening of the time period over which innovation statistics are sampled (Figure 7). In contrast, a sharp improvement in convergence is noted when the Mehra approach is constrained to predict only physically realistic values of Q (Figure 8). This improvement, however, reduces the fidelity of the approach with regards to cases in which Q_{true} and R_{true} are not approximately equal (Figure 9). In an operational setting, the only effective strategy for improving the convergence of the Mehra approach may be to assume R_{true} is known and limit the adaptive filtering retrieval to the estimation of Q_{true} only (Figure 8).

[51] The nudge whitening and Desroziers approaches appear to provide viable alternatives to the Mehra approach. In particular, both approaches provide faster adaptive convergence at a cost of only minor reductions in long-term accuracy (Figure 5). These empirical approaches may also be better suited to implementation within an EnKF-based land data assimilation system than the closed form Mehra approach. Land surface model error in an EnKF implementation is commonly introduced via Monte Carlo–based variations in forcing data and model parameter, in addition to (or instead of) the direct perturbation of state vectors captured by $\mathbf{Q}$. Consequently, the analytical calculation of $\mathbf{Q}$ by the Mehra approach may not be of direct value for efforts to constrain the magnitude of model uncertainty

induced indirectly via noise in model forcings and/or parameter selection. In contrast, the more flexible iterative nature of the empirical approaches (i.e., nudge whitening and Desroziers) can be applied to tune any type of modeling error chosen to generate the EnKF Monte Carlo ensemble. This potential benefit, however, must be weighed against parameterization issues facing these empirical approaches. In particular, the *Reichle et al.* [2008] implementation of the Desroziers approach requires a fairly complex parameterization. Of particular concern is the β parameter introduced by *Reichle et al.* [2008] and its impact on Desroziers adaptive filtering results (Figure 10).

[52] Despite progress made here, our analysis is limited by several factors that could be addressed in future work. First, by assuming α and ρ parameters in **Q** are known (see section 2.2), we focus only on the estimation of model error magnitudes. In reality a number of additional model error parameters describing the vertical, lateral and temporal autocorrelation of model error will need to be constrained. In addition, a more general analysis would examine a broader range of land surface observations including remotely sensed snow and land surface temperature. Finally, the point-scale nature of the study prevents us from examining the impact of variations in land cover and/or micrometeorological conditions on the performance of various adaptive filters. Additional work addressing any of these limitations would likely prove worthwhile.

[53] **Acknowledgments.** Partial support for this study was provided through NASA grant NNG05GB61G.

References

Burgers, G., P. J. van Leeuwen, and G. Evensen (1998), Analysis scheme in the ensemble Kalman filter, *Mon. Weather Rev.*, *126*, 1719–1724.

Cosby, B. J., G. M. Hornberger, R. B. Clapp, and T. R. Ginn (1984), A statistical exploration of the relationships of soil moisture characteristics to the physical properties of soils, *Water Resour. Res.*, *20*, 682–690.

Crow, W. T., and J. D. Bolten (2007), Estimating precipitation errors using spaceborne surface soil moisture retrievals, *Geophys. Res. Lett.*, *34*, L08403, doi:10.1029/2007GL029450.

Crow, W. T., and E. Van Loon (2006), Impact of incorrect model error assumptions on the sequential assimilation of remotely sensed surface soil moisture, *J. Hydrometerol.*, *7*, 421–432.

Crow, W. T., and E. F. Wood (2003), The assimilation of remotely sensed soil brightness temperature imagery into a land surface model using ensemble Kalman filtering: A case study based on ESTAR measurements during SGP97, *Adv. Water Resour.*, *26*, 137–149.

Crow, W. T., W. P. Kustas, and J. Prueger (2008), Monitoring root-zone soil moisture through the assimilation of a thermal remote sensing-based soil moisture proxy into a water balance model, *Remote Sens. Environ.*, *112*, 1268–1281.

Dee, D. P. (1995), On-line estimation of error covariance parameters for atmospheric data assimilation, *Mon. Weather Rev.*, *123*, 1128–1145.

Desroziers, G., L. Berre, B. Chapnik, and P. Poli (2005), Diagnosis of observation, 10 background and analysis-error statistics in observation space, *Q. J. R. Meteorol. Soc.*, *131*, 3385–3396, doi:10.1256/qj.05.108.

Dirmeyer, P. A., A. J. Dolman, and N. Sato (1999), The pilot phase of the Global Soil Wetness Project, *Bull. Am. Meteorol. Soc.*, *80*, 851–878.

Drusch, M. (2007), Initializing numerical weather prediction models with satellite-derived surface soil moisture: Data assimilation experiments with ECMWF's Integrated Forecast System and the TMI soil moisture data set, *J. Geophys. Res.*, *112*, D03102, doi:10.1029/2006JD007478.

Evensen, G. (1994), Sequential data assimilation with a nonlinear quasi-geostrophic model using Monte Carlo methods to forecast error statistics, *J. Geophys. Res.*, *99*, 10,143–10,162.

Gelb, A. (1974), *Applied Optimal Estimation*, 374 pp., MIT Press, Cambridge, Mass.

Gish, T. J., C. L. Walthall, C. S. T. Daughtry, and K.-J. S. Kung (2005), Using soil moisture and spatial yield patterns to identify subsurface flow pathways, *J. Environ. Qual.*, *34*, 274–286.

Jackson, T. J. (1993), Measuring surface soil moisture using passive microwave remote sensing, *Hydrol. Processes*, *7*, 139–152.

Mehra, R. K. (1970), On identification of variances and adaptive Kalman filtering, *IEEE Trans. Automatic Control*, *2*, 175–184.

Mitchell, H. L., and P. L. Houtekamer (1999), An adaptive ensemble Kalman filter, *Mon. Weather Rev.*, *128*, 416–433.

Montaldo, N., J. D. Albertson, M. Marcini, and G. Kiely (2001), Robust prediction of root zone soil moisture from assimilation of surface soil moisture, *Water Resour. Res.*, *37*, 2889–2900.

Noilhan, J., and S. Planton (1989), A simple parameterization of land surface processes in meteorologic models, *Mon. Weather Rev.*, *117*, 536–549.

Norman, J. M., W. P. Kustas, and K. S. Humes (1995), A two-source approach for estimating soil and vegetation energy fluxes in observations of directional radiometric surface temperature, *Agric. For. Meteorol.*, *77*, 263–293.

Reichle, R. H., and R. D. Koster (2002), Land data assimilation with the ensemble Kalman filter: Assessing model error parameters suing innovations, in *Proceedings of the XIV International Conference on Computational Methods in Water Resources*, edited by S. M. Hassanizadeh et al., pp. 1387–1394, Elsevier, New York.

Reichle, R. H., and R. D. Koster (2003), Assessing the impact of horizontal error correlations in background fields on soil moisture estimation, *J. Hydrometeorol.*, *4*, 1229–1242.

Reichle, R. H., and R. D. Koster (2005), Global assimilation of satellite surface soil moisture retrievals into the NASA Catchment land surface model, *Geophys. Res. Lett.*, *32*, L02404, doi:10.1029/2004GL021700.

Reichle, R. H., D. B. McLaughlin, and D. Entekhabi (2002), Hydrologic data assimilation with the ensemble Kalman filter, *Mon. Weather Rev.*, *130*, 103–114.

Reichle, R. H., R. D. Koster, P. Liu, S. P. P. Mahanama, E. G. Njoku, and M. Owe (2007), Comparison and assimilation of global soil moisture retrievals from the Advanced Microwave Scanning Radiometer for the Earth Observing System (AMSR-E) and the Scanning Multichannel Microwave Radiometer (SMMR), *J. Geophys. Res.*, *112*, D09108, doi:10.1029/2006JD008033.

Reichle, R. H., W. T. Crow, and C. L. Keppenne (2008), An adaptive ensemble Kalman filter for soil moisture data assimilation, *Water Resour. Res.*, *44*, W03423, doi:10.1029/2007WR006357.

Rodell, M. A., et al. (2005), The Global Land Data Assimilation System, *Bull. Am. Meteorol. Soc.*, *85*, 381–394, doi:10.1174/BAMS-85-3-381.

Walker, J. P., and P. R. Houser (2001), A methodology for intializing soil moisture in a global climate model: Assimilation of near-surface soil moisture observations, *J. Geophys. Res.*, *106*, 11,761–11,774.

Yates, D. N., F. Chen, and H. Nagai (2003), Land surface heterogeneity in the Cooperative Atmosphere Surface Exchange Study (CASES-97). Part II: Analysis of spatial heterogeneity and its scaling, *J. Hydrometeorol.*, *4*, 219–234.

W. T. Crow, Hydrology and Remote Sensing Laboratory, Agricultural Research Service, U.S. Department of Agriculture, Room 104, Building 007, BARC-W, Beltsville, MD 20705, USA. (wade.crow@ars.usda.gov)

R. H. Reichle, Global Modeling and Assimilation Office, Goddard Earth Sciences and Technology Center, NASA Goddard Space Flight Center, Greenbelt, MD 20771, USA.